Available online at www.eccomasproceedia.org
Eccomas Proceedia COMPDYN (2023) 900-924

ECCOMAS
Proceedia

COMPDYN 2023
9th ECCOMAS Thematic Conference on
Computational Methods in Structural Dynamics and Earthquake Engineering
M. Papadrakakis, M. Fragiadakis (eds.)
Athens, Greece, 12-14 June 2023

PREDICAMENT OF THE 1D ASSUMPTION IN SITE RESPONSE ANALYSIS AND IMPLICATIONS FOR VERTICAL GROUND MOTION ASSESSMENT

Junfei Huang[1], **David McCallen**[2]

[1] University of Nevada, Reno
1664 N Virginia St, Reno, NV 89557
e-mail: jfhuang@nevada.unr.edu

[2] University of Nevada, Reno
1664 N Virginia St, Reno, NV 89557
[2] Lawrence Berkeley National Laboratory
One Cyclotron Road, Berkeley, CA 94720
e-mail: dmccallen@unr.edu

Abstract

In one-dimensional site response analysis (1D SRA), the horizontal and vertical ground motions are assumed to be induced by vertically propagating shear and compressional waves, respectively. Although this 1D assumption is utilized as a standard practice in site-specific ground motion estimation, its applicability to realistic seismic wavefields is still in question. There is special concern for vertical ground motion assessment, as vertical motions predicted by this 1D approach have tended to be consistently larger than field observations. In this paper, we evaluate the accuracy and implications of 1D SRA when applied to general inclined seismic wavefields. Based on the analytical solution of inclined P-SV waves, two observed deficiencies inherent in this 1D approach, namely, the systematic over-prediction of the vertical motion and excessively long-duration motions predicted with the in-column input motion, are identified, and corresponding physical explanations are provided. It is shown that the over-prediction of the vertical motion is a result of the inability of the 1D approach to account for the refraction of the large-amplitude SV waves when propagating through the surficial soft layers, and is more pronounced for soil profiles with a strong soil velocity gradient. The phenomenon of excessively long-duration motions is incurred by the enforced fixed boundary at the 1D soil column base that is unable to represent the outgoing waves. These observations are further confirmed using simulated ground motions from three-dimensional regional-scale earthquake simulations performed on massively parallel computers. The analysis results suggest that the vertical amplification mechanism is fundamentally different from that assumed in the simplified 1D approach, and inclined shear waves should be accounted for when selecting vertical input motions for engineering applications.

Keywords: Site Response Analysis, 1D Assumption, Vertical Ground Motion, Wave Propagation, Inclined Seismic Wave, Ground Motion Simulation.

ISSN:2623-3347
Peer-review under responsibility of the organizing committee of COMPDYN 2023.
doi: 10.7712/120123.10445.21275

1 INTRODUCTION

In geotechnical earthquake engineering and engineering seismology, one of the essential tasks is to assess the earthquake-induced ground shaking considering the near-surface soil conditions and to obtain site-specific design ground motions for critical infrastructures [1]. Since the pioneering works in the 1950s~70s, e.g. [2–4], one-dimensional site response analysis (1D SRA) is used by the majority of existing site response studies and is the standard practice in predicting the local site response. In 1D SRA, it is assumed that the surficial soils are horizontally layered and the seismic waves are nearly vertically propagating when approaching the ground surface due to wave refraction in the soft soil layers, and in this context, the horizontal and vertical motions can be represented by vertically propagating shear and compressional waves, respectively, which are collectively known as the 1D assumption.

Although 1D SRA has seen wide applications, its applicability to realistic seismic wavefield is still in question. With the increasingly available recorded ground motions over the past decades, investigations are being carried out to test the validity of the 1D assumption in predicting the horizontal motions. Recent studies on horizontal motions utilizing recorded data from vertical downhole arrays have shown that deviation of real-world site response from the 1D assumption is common. For example, Thompson et al. [5] studied 104 downhole arrays in the KiK-net strong-motion network in Japan and concluded that only 16 sites resembled one-dimensional response based on low inter-event variability and good fit to the theoretical 1D transfer function. Pilz and Cotton [6] found 45% of the selected 354 KiK-net sites were influenced by 2D and 3D effects. In addition, vertical motions predicted by the 1D approach have been observed to be consistently larger than field observations. Elgamal and He [7] employed a 1D vertical P wave propagation model to predict the vertical response of the Lotung downhole array in Taiwan and found that approximately 25% reduction in the P wave velocity and unphysically high damping (15-25%, even for small tremors) was required in the model for a good match with the recorded data. This is in agreement with findings by Mok et al [8]. A similar optimization procedure was applied to the five downhole array profiles studied by Tsai and Liu [9] and different levels of velocity reduction and damping increase were used to calibrate the vertical response on a site-to-site basis. As a result, 1D SRA for vertical ground motion prediction is considered unreliable and various adjustments based on the empirical vertical-to-horizontal (V/H) spectral ratios are commonly used in current design standards and regulatory guidelines [10–14].

Seismic waves incurred by real earthquakes are rarely vertically propagating considering the finiteness of the rupturing fault, the complex wave propagation phenomena in the heterogeneous subspace, and the geometrical orientation between the earthquake source and the site of interest. This is especially of importance to vertical ground motion assessment, since in contrast to the vertical P wave propagation assumed in 1D SRA, inclined large-amplitude S waves can lead to significant vertical components that may dominate the vertical site response, even at small incident angles. Chao et al. [15] reported that approximately 73% of the 37,888 strong vertical motion records observed in Taiwan for both crustal and subduction earthquakes are classified as S-dominated, i.e., the peak vertical acceleration occurs within the S wave window, suggesting the strong correlation between the peak vertical motion and S waves. To date, although the question of S wave contribution to the vertical motion has been raised, the extent to which it affects the vertical site response, particularly its connection with the field observation of over-prediction of the vertical motion by 1D SRA, remains unclear and needs further investigation.

In this paper, we evaluate the accuracy and implications of 1D SRA when applied to general inclined seismic wavefields. For this purpose, we base our study mainly on high-fidelity

simulated ground motions to avoid the uncertainties in site characterization, soil modeling, and input motion selection that are commonly observed in previous site response studies [5,9,16]. For rigorous evaluation of the 1D wave propagation assumption, it is recognized that extensive numerical investigations grounded on realistic broadband three-dimensional (3D) earthquake simulations should be used. Although this capability is becoming realized with the emerging next-generation high-performance computing platforms, e.g., [17,18], as in any type of analysis, a simplified analytical approach can be useful in exploring the large parameter space and informing important aspects that need to be captured in the computationally intensive full 3D earthquake simulations. At sufficiently large distances from the earthquake source, the curvature of the incoming spherical wavefronts is relatively small and the seismic waves arriving at a local engineering site can, to the first order, be well represented by inclined plane waves [19]. For the purpose of this study, as the reference true site response solutions, we utilize both analytical 2D inclined plane P-SV waves and realistic seismic wavefields from broadband fully deterministic 3D ground motion simulations.

In the following sections, we first present the methods to obtain the reference inclined seismic waves, including the analytical solution for inclined 2D plane waves propagating in multilayered media and 3D fourth-order finite difference ground motion simulations for representative basin models. We then report the performance of 1D SRA through detailed comparisons between the 1D SRA predictions and reference solutions from both analytical 2D plane waves and 3D ground motion simulations. Deficiencies inherent in this 1D approach, namely, the systematic over-prediction of the vertical motion and excessively long-duration motions predicted with the in-column input motion, are identified. Physical explanations and representative examples are also provided. Evidence of the identified deficiencies and implications for regional-scale seismic hazard and risk assessment are further emphasized.

2 METHODS FOR DEVELOPMENT OF REFERENCE 2D AND 3D SITE RESPONSE

2.1 Analytical inclined P-SV waves propagating in viscoelastic layered media for 2D site response

In this section, we summarize the development and implementation of the analytical inclined P-SV waves used in this study and provide verification examples. This analytical approach enables us to examine the accuracy of the 1D approach when applied to representative inclined plane waves propagating in multilayered media with different material properties and at different incident angles, with the advantage of separating the influence of incoming incident P and S waves that coexist in real earthquake records.

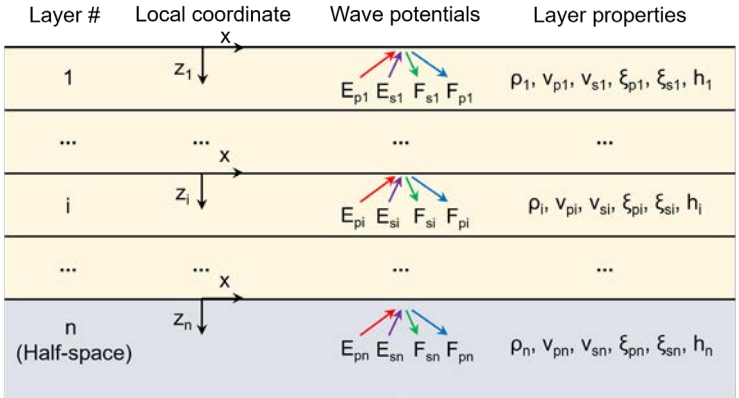

Figure. 1. Properties of the layered viscoelastic media and wave potentials for incident and reflected P-SV waves. Layer properties include the density ρ, P and S wave velocities v_p and v_s, P and S wave damping ratios ξ_p and ξ_s, and layer thickness h.

2.1.1 Development and implementation

We generally follow the frequency-domain formulation presented by Zhao et al. [20] for elastic P-SV waves at incident angles less than the critical angle. Since seismic waves are attenuated when propagating through all real materials and the incident angle is site dependent, we extend the formulation to include realistic energy dissipation due to viscoelasticity, and to include plane waves beyond the critical angle of incidence. These are realized by considering complex elastic moduli and wave velocities for the layer materials, and complex incident and reflection angles for the plane waves.

For a layered viscoelastic media as shown in Figure 1, the wave potential functions ϕ_i for plane P waves and ψ_i for plane SV waves that satisfy the wave equations in layer i can be expressed in the frequency domain as

$$\begin{aligned} \phi_i &= E_{pi}\exp[j\omega(px - q^i_{pz} z_i - t)] + F_{pi}\exp[j\omega(px + q^i_{pz} z_i - t)] \\ \psi_i &= E_{si}\exp[j\omega(px - q^i_{sz} z_i - t)] + F_{si}\exp[j\omega(px + q^i_{sz} z_i - t)] \end{aligned} \tag{1}$$

where E_{pi}, E_{si}, F_{pi} and F_{si} are the wave potential amplitudes for the incident P, incident SV, reflected P, and reflected SV waves in the layer, respectively; p is the horizontal slowness; q^i_{pz} and q^i_{sz} are the vertical slownesses for P and SV waves, respectively; ω is the circular frequency; and j is the imaginary unit. The horizontal and vertical slownesses for layer i are calculated by

$$\begin{gathered} p = \frac{\sin\alpha_i}{v_{pi}} = \frac{\sin\beta_i}{v_{si}} \\ q^i_{pz} = \frac{\cos\alpha_i}{v_{pi}} = \sqrt{\left(\frac{1}{v_{pi}}\right)^2 - p^2},\ q^i_{sz} = \frac{\cos\beta_i}{v_{si}} = \sqrt{\left(\frac{1}{v_{si}}\right)^2 - p^2} \end{gathered} \tag{2}$$

where α_i and β_i are the incident angles between the wave propagation direction and the vertical axis for P and SV waves, respectively. It is noted that we have adopted a sign convention for the Fourier transform in eq. (1) that is different from the original formulation by Zhao et al. [20] and eq. (2) is suitable for both under- and super-critical incident angle cases of elastic plane waves [19].

To incorporate equivalent viscous damping for wave attenuation in the system, we consider the Kelvin-Voigt rheological model for the materials and compute the horizontal and vertical slownesses in eq. (2) using complex-valued wave velocities as follows [21]

$$v^*_{pi} = \sqrt{\frac{M_i^*}{\rho_i}} = \sqrt{\frac{(\lambda_i + 2\mu_i)^*}{\rho_i}},\ v^*_{si} = \sqrt{\frac{\mu_i^*}{\rho_i}} \tag{3}$$

where $M_i^* = (\lambda_i + 2\mu_i)^* = (\lambda_i + 2\mu_i)(1 - 2\xi_{pi} j)$ and $\mu_i^* = \mu_i(1 - 2\xi_{si} j)$ are the complex constrained and shear moduli, respectively, and λ, μ are the elastic Lamé constants. For viscoelastic waves, the quantities in the square roots in eq. (2) are complex numbers and the sign of the vertical slowness cannot be determined by the radiation condition at the layer interface as in the elastic case. Following the method proposed by Krebes and Daley [22], we use the real part of the horizontal slowness in the evaluation of q_{pz} and q_{sz} to obtain continuous and elastically consistent viscoelastic waves.

The displacement and stress vector $\boldsymbol{y}_i(x, z_i)$ within layer i can be expressed as

$$\boldsymbol{y}_i(x, z_i) = [u^i_x,\ u^i_z,\ \sigma^i_{zz},\ \tau^i_{xz}]^T \exp[j\omega(px - t)] = \boldsymbol{Q}_i \boldsymbol{d}_i(z_i) \boldsymbol{E}_i \exp[j\omega(px - t)] \tag{4}$$

where

$$\boldsymbol{Q}_i = \begin{bmatrix} j\omega p & j\omega p & j\omega q_{sz}^i & -j\omega q_{sz}^i \\ -j\omega q_{pz}^i & j\omega q_{pz}^i & j\omega p & j\omega p \\ P_i & P_i & 2\mu_i^* \omega^2 p q_{sz}^i & -2\mu_i^* \omega^2 p q_{sz}^i \\ 2\mu_i^* \omega^2 p q_{pz}^i & -2\mu_i^* \omega^2 p q_{pz}^i & \eta_i & \eta_i \end{bmatrix}$$

$$P_i = -\lambda_i^* \omega^2 p^2 - (\lambda_i^* + 2\mu_i^*)\omega^2 (q_{pz}^i)^2$$

$$\eta_i = \mu_i^* \omega^2 [(q_{sz}^i)^2 - p^2],\ \lambda_i^* = \rho_i [(v_{pi}^*)^2 - 2(v_{si}^*)^2]$$

$$\boldsymbol{E}_i = [E_{pi},\ F_{pi},\ E_{si},\ F_{si}]^T$$

$$\boldsymbol{d}_i(z_i) = \mathrm{diag}(\exp(-j\omega q_{pz}^i z_i),\ \exp(j\omega q_{pz}^i z_i),\ \exp(-j\omega q_{sz}^i z_i),\ \exp(-j\omega q_{sz}^i z_i))$$

Considering the stress-free surface condition, the normal stress σ_{zz}^1 and shear stress τ_{xz}^1 on the ground surface are zero, which gives

$$\begin{aligned} \sigma_{zz}^1(\forall x, 0) &= P_1(E_{p1} + F_{p1}) + 2\mu_1^* \omega^2 p q_{sz}^1 (E_{s1} - F_{s1}) = 0 \\ \tau_{xz}^1(\forall x, 0) &= 2\mu_1^* \omega^2 p q_{pz}^1 (E_{p1} - F_{p1}) + \eta_1 (E_{s1} + F_{s1}) = 0 \end{aligned} \tag{5}$$

It is worth noting that for the special case where there is only one layer in the system (i.e., half-space), if either of the two surface motions (u_x, u_z) or the two incident wave amplitudes (E_p, E_s) are known, the six expressions in eqs. (4-5) relating the remaining six unknowns can be solved. For a multilayered system, however, we derive the recursive expression relating the wave potentials in the top layer and the bottom half-space based on the continuity of displacements and stresses at the layer interfaces, i.e., $\boldsymbol{y}_i(x, h_i) = \boldsymbol{y}_{i+1}(x, 0)$, as

$$\boldsymbol{E}_n = \prod_{i=n-1}^{1} \boldsymbol{T}_i \boldsymbol{E}_1 \tag{6}$$

where T_i is the transfer matrix for wave potentials of adjacent layers and can be written as

$$\boldsymbol{T}_i = \boldsymbol{Q}_{i+1}^{-1} \boldsymbol{Q}_i \boldsymbol{d}_i(h_i) \tag{7}$$

Eqs. (5-7) provide six equations relating the eight wave potential amplitude unknowns in $\boldsymbol{E}_1$ and $\boldsymbol{E}_n$. To solve for the free-field response, two additional equations can be obtained based on the characteristics of the input motion. In this study, we consider two types of input motions that are commonly used in site response analysis, i.e., input motions recorded at rock outcrops and input motions recorded below the ground surface (hereafter referred to as the outcrop and in-column motions, respectively).

In the first case, the outcrop motions are known. The incident P and SV waves can be obtained by solving the one-layered half-space problem as mentioned earlier. For vertically propagating waves (as assumed in 1D SRA), the incident P and SV waves can be taken as half of the outcrop motions accounting for the free-surface amplification effect. The wave potential amplitude and the incident wave displacement are related by

$$E_{pn} = -j \frac{\overline{u}_p v_{pn}^*}{\omega \exp(j\omega p x_{ref})},\ E_{sn} = -j \frac{\overline{u}_s v_{sn}^*}{\omega \exp(j\omega p x_{ref})} \tag{8}$$

where $\overline{u}_p$ and $\overline{u}_s$ are the known Fourier displacement amplitudes of incident P and SV waves in the half-space, respectively, and x_{ref} is the horizontal reference location on top of the half-space for the incident motions.

In the second case, the in-column motions induced by the incident P and SV waves at a reference depth, e.g., the top of the half-space as assumed in this study, are known, which gives

$$\begin{aligned} \overline{u}_x &= j\omega p(E_{pn} + F_{pn}) + j\omega q_{sz}^n (E_{sn} - F_{sn}) \\ \overline{u}_z &= -j\omega q_{pz}^n (E_{pn} - F_{pn}) + j\omega p(E_{sn} + F_{sn}) \end{aligned} \tag{9}$$

where $\overline{u}_x$ and $\overline{u}_z$ are the known Fourier amplitudes of the horizontal and vertical displacements on top of the half-space. Based on eqs. (5-9), $\boldsymbol{E}_1$ and $\boldsymbol{E}_n$ can be solved, and the wave potentials in the remaining layers can be calculated using eq. (6). The wave amplitude at each frequency for displacement, velocity, and acceleration responses in the system can then be calculated using eq. (4) and the wave motions in the time domain can be computed based on the inverse Fourier transform.

For efficient computation of the general inclined plane wavefields, and comparison with 1D SRA results, we implemented the preceding formulation in a recently developed Python code, Site2D, with command line interface and visualization capabilities. To achieve optimal efficiency for solving plane waves propagating in a single large computational domain or processing multiple sites in parallel, the calculation process for each frequency is parallelized with the *multiprocessing* module [23] and further speedup is obtained through the translation to machine code at run time by the *Numba* just-in-time (JIT) compiler [24]. Although plane waves are 2D motions by nature (i.e., motions are independent of the spatial location in the out-of-plane direction), seismic motions in 3D space can be obtained by specifying appropriate coordinate system transformation in Site2D when applied to 3D engineering systems [25,26].

2.1.2 Verification

We present two cases to verify the implementation of the analytical plane waves in the Site2D program by inter-code comparison and representative results in the literature.

In the first case, inclined P and SV waves propagating in an example soil site, as shown in Table 1, at incident angles of 60° and 27.6°, respectively, are considered. This problem was studied by Wolf and Obernhuber [27] using the stiffness matrix method. Figure 2 shows the horizontal and vertical amplification factors calculated between the surface motion and the corresponding outcrop motion (i.e., with the soil layers above the half-space removed) for the two plane wave cases. As can be seen, good agreements are obtained between Site2D used in this study and the reference solutions.

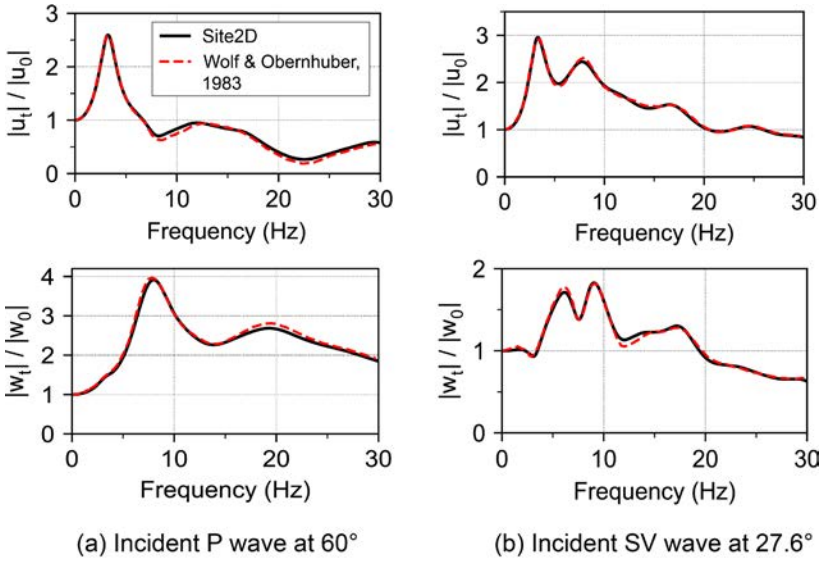

Figure. 2. Horizontal (top) and vertical (bottom) amplification factors between surface and outcrop motions for (a) inclined P wave with incident angle as 60°; and (b) inclined SV wave with incident angle as 27.6°.

Layer	Mass density (kg/m^3)	Wave velocity (m/s)		Damping ratio		Thickness (m)
		P wave	S wave	P wave	S wave	
1	2000	490	200	0.07	0.07	5
2	2000	612	250	0.06	0.06	5
3	2000	857	350	0.05	0.05	10
4	2200	1225	500	0.05	0.05	10
5	2200	1960	800	0.05	0.05	10
6	2400	2082	1000	0.04	0.04	10
7	2500	2806	1500	0.02	0.02	-

Table 1. Soil properties of the selected soil profile [27]

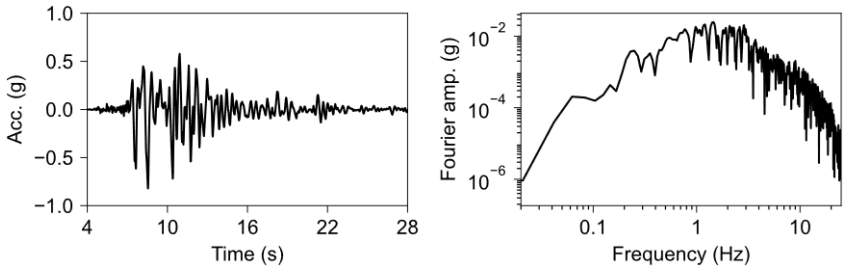

Figure. 3. Kobe input acceleration and Fourier amplitude spectrum

In the second example, we consider a special case where shear waves are vertically propagating in the selected soil profile (Table 1). Since the wave is vertically propagating, the results can be compared to that modeled by existing 1D codes. Both outcrop and in-column input motion conditions are tested using the input signal from the 1995 Kobe earthquake (Figure 3). Figure 4 shows the comparison of horizontal ground responses between the frequency-domain solutions from Site2D and DEEPSOIL [28], and the time-domain solution from OpenSees [29]. Although small discrepancies exist between the frequency- and time-domain solutions due to differences in element formulation and the respective damping mechanisms, the results provide confidence in the implementation of the analytical plane wave solution in Site2D.

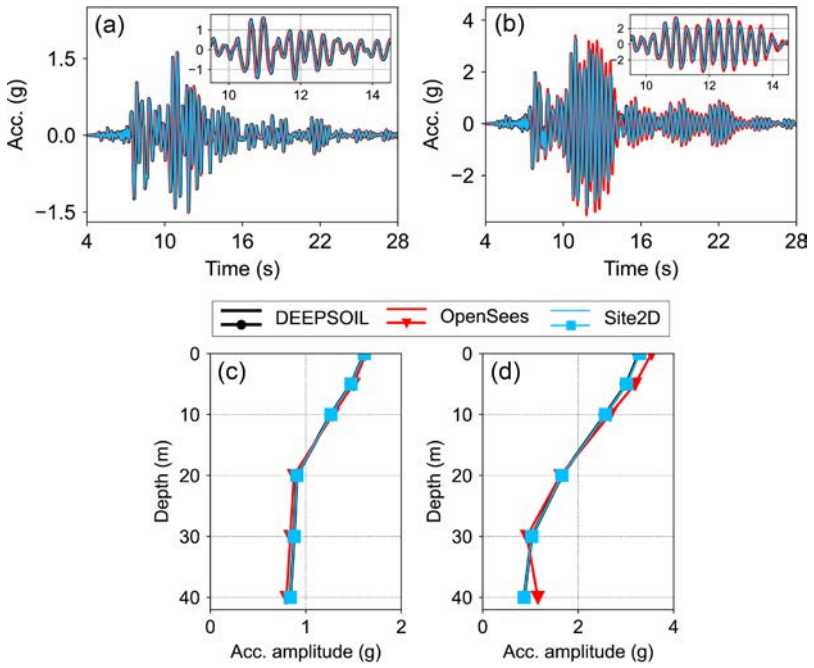

Figure. 4. Comparison of surface acceleration (top row) and acceleration amplitude along depth (bottom row) calculated by DEEPSOIL, OpenSees and Site2D for the selected soil profile (Table 1) assuming the input motion (Figure 3) as the outcrop motion in (a) and (c), and as the in-column motion in (b) and (d).

2.2 High-order finite difference numerical simulation for 3D site response

We employed fully deterministic 3D earthquake simulations to obtain spatially-dense high-fidelity ground motions as input motions and reference true 3D solutions for comparison with the 1D analyses. Compared to hybrid simulations that combine deterministic motions at low frequencies with high-frequency motions from a stochastic method to relax the computational requirements, this fully deterministic approach preserves the 3D wave propagation mechanics across a broad frequency range which is essential for the purpose of this study [30]. The simulations were performed using SW4 (Seismic Waves, 4th order), a finite difference code with fourth-order accuracy in space and time for viscoelastic seismic wave propagation and highly optimized for regional-scale earthquake simulations [17,31]. In this work, we consider seismic waves in regional generic basin models induced by both an idealized point earthquake source and a representative extended source for a Mw 6.5 strike-slip earthquake event through explicit modeling of the rupture process. In view of the fact that the real fault rupture process is frequently modeled as spatially distributed point sources, the simple point source scenario allows us to examine the relative contribution of the incident P and S waves to the total wavefield without the complications created by complex interferences of seismic waves emitted from different locations. To cover a broad frequency range that is of interest to engineering applications, our ground motions are resolved to a maximum frequency of 5Hz with at least eight grid points per wavelength. The numerical simulations were run on the Cori supercomputer [32] given the significant computational requirements.

For the point source case, we utilized the computational domain and material properties as shown in Figure 5. For simplicity, all materials have the same mass density ρ=2178kg/m^3, Poisson's ratio ν=0.31, with quality factor Q for P wave twice as that for the S wave. The damping ratio ξ is related to Q by ξ=1/2Q. The wave velocities increase linearly with depth in the sedimentary basin while the rock is homogeneous in the domain. Considering the north direction is aligned with the local x axis in SW4 (Figure 5), we use a dip-slip source located at 6km depth with strike, dip, and rake angles as 90°, 60°, and 90°, respectively, which results in incident P and SV waves polarized primarily along the vertical plane coinciding with the middle dashed line in the domain where simulated ground motions are recorded.

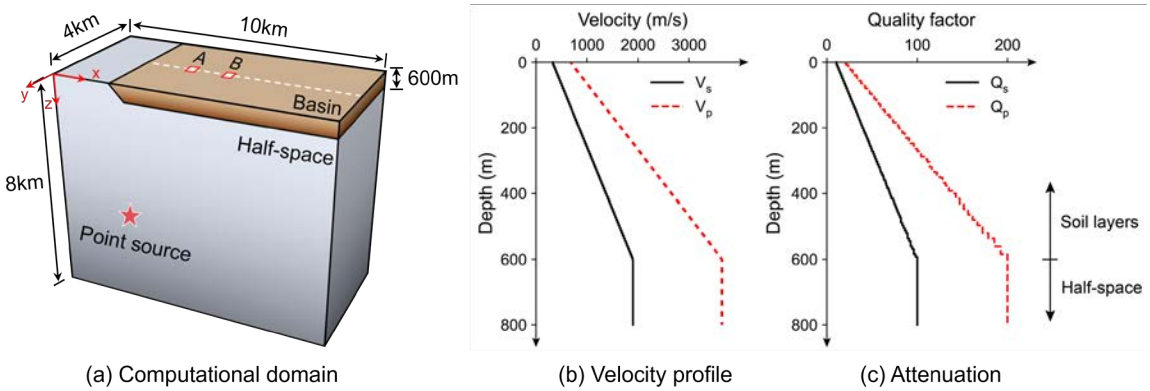

(a) Computational domain (b) Velocity profile (c) Attenuation

Figure. 5. Ground motion simulation of a point earthquake source scenario: (a) computational domain in SW4, (b) velocity profile, and (c) attenuation property. The ground motions are recorded along the middle dashed line in the sedimentary basin.

For the Mw 6.5 strike-slip event, the generic regional domain consists of a layered crustal model and a shallow sedimentary basin along a vertical fault rupture plane and is considered to be representative of the geologic environment of common shallow crustal earthquakes in active tectonic regimes. The computational domain used in this study is 44km×20km span-

ning in the horizontal directions and 25km in depth encompassing the vertical 27km×12km rectangular rupture plane determined based on empirical relations between seismic moment and fault area for strike-slip events, as shown in Figure 6. Note for this event, we have chosen a basin model that has a strong impedance contrast (~2.7 for shear waves) at the base of the basin to reflect the possible discontinuity in the material properties. The fault rupture process is modelled using the Grave-Pitarka kinematic rupture model [33], where the rupture plane is divided into a number of smaller subfaults described by spatially varying rupture characteristics including the slip, rise time, and rake direction. The rupture velocity is constrained to be approximately 80 percent of the local shear wave velocity and the hypocenter is placed on the left side of the fault. In this way, complex wave propagation phenomena in 3D geologic structure and important near-fault directivity effects and permanent displacements can be captured in the ground motion simulations. To examine the spatial variability in the performance of the 1D approach in predicting the horizontal and vertical ground responses, the input and reference true ground motions were obtained on a 1km×1km surface grid on the basin side, resulting in a total of 602 sites used in the 1D SRA.

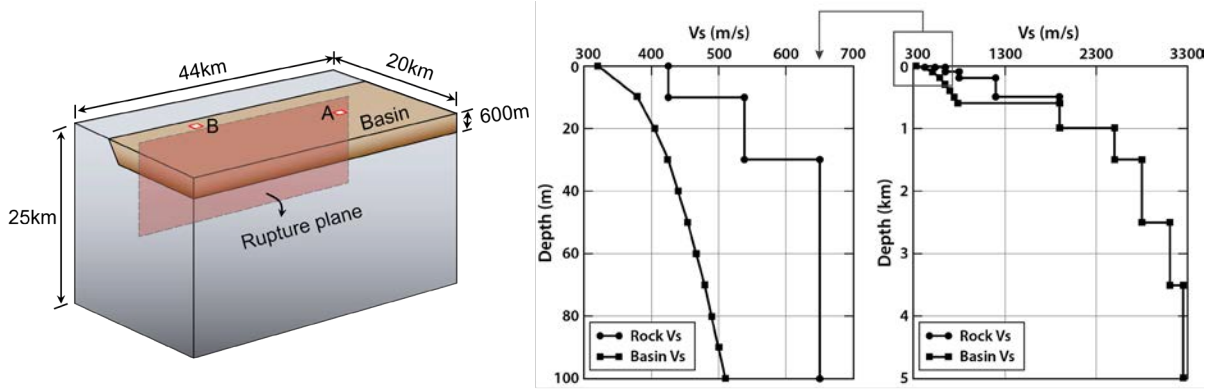

(a) Computational domain

(b) Velocity profile at rock and basin sites

Figure. 6. Ground motion simulation of a Mw 6.5 strike-slip event in SW4: (a) computational domain, and (b) velocity profile at rock and basin sites

2.3 1D site response analysis

In this study, we conducted 1D SRA for both analytical 2D wavefields and realistic seismic waves from 3D ground motion simulations. The soil columns and input motions for 1D SRA were obtained from the corresponding 2D and 3D wavefields to be consistent with the expectation in practice. The base of the soil column was chosen at the top of the half-space or the rock-basin interface (i.e., 600m depth). As mentioned in the introduction, S waves dominate the horizontal motions and may contribute significantly to the vertical ground response. In the calculation of the 2D plane wavefields, to examine the implications for vertical site response estimation when applying the simplified 1D approach, we considered only incident S waves from the half-space. For demonstration purposes, we used the soil profile with linear velocity gradient (Figures 5b and 5c) with the incident S wave signal defined by a narrow-band Ricker wavelet (eq. (10)) with central frequency f_c=10Hz.

$$\ddot{u}(t) = (2\pi^2 f_c^2 t^2 - 1)\exp(-\pi^2 f_c^2 t^2) \tag{10}$$

Two types of input motions were used to excite the 1D soil column, as shown in Figure 8. The in-column motions were the total motions recorded at the base of the soil layers in a horizontally layered system or at the rock-basin interface in the generic basin models. The outcrop motions consisted of the surface motions recorded on rock in a complementary analysis where

surficial soil layers or basin were removed while the remaining model was subjected to the same incident wavefield. Note since the geologic model and source-to-site distance were preserved in the complementary analysis, uncertainties induced by amplitude scaling of the outcrop input motions required when using actual records are avoided [4]. Assuming vertically propagating waves, we used half of the recorded outcrop motions as the incident waves in the 1D analyses.

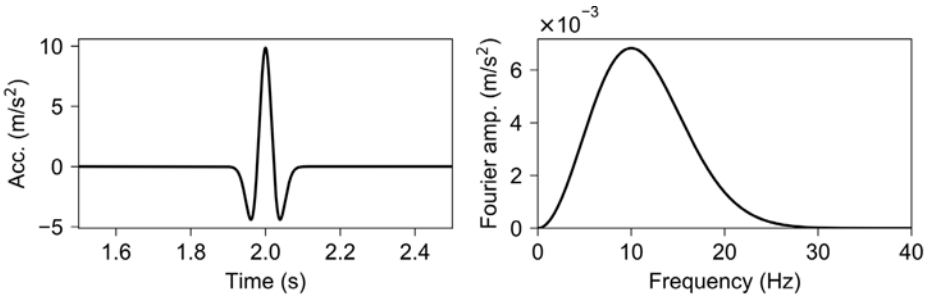

Figure. 7. Ricker wavelet input acceleration and Fourier amplitude spectrum

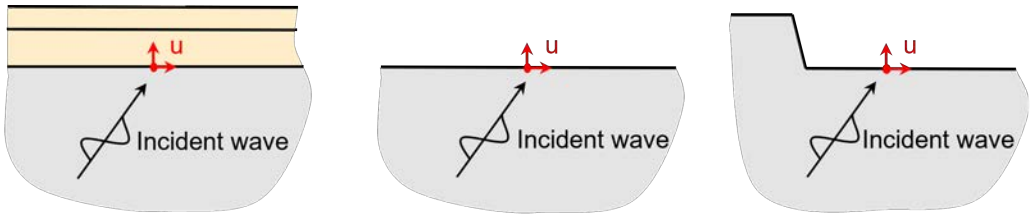

(a) In-column motion (b) Outcrop motion

Figure. 8. Input motions *u* for 1D SRA: (a) in-column motion at the base of the soil layers, (b) outcrop motion on the surface of the rock with overlying soil layers removed (left) and basin removed (right)

For computational efficiency, all the 1D site response analyses were performed using the command line interface of Site2D. The applicability of 1D SRA, including the prediction bias and spatial variability, is evaluated through detailed comparisons between the ground responses predicted by 1D SRA and reference solutions from the analytical 2D wavefields and 3D earthquake simulations, as discussed in the following sections.

3 ASSESSMENT OF 1D SRA COMPARED TO REFERENCE TWO-DIMENSIONAL GROUND MOTION SIMULATIONS

3.1 Over-prediction of the vertical motion

First, we present the analysis results for a simple case where the seismic waves are vertically propagating in the horizontally layered system, i.e., incident angle β of the SV wave from the underlying half-space is 0°. This case satisfies the 1D assumption and serves as a baseline verification example. Figure 9 shows the comparison of horizontal surface accelerations computed by the reference 2D plane wave solution and by 1D SRA with both types of input motions. Figure 10 shows snapshots of the actual 2D reference wavefield and 1D wavefields predicted by 1D SRA, at four instants in time, starting from the incident S wave first entering and then leaving the soil domain. As expected, the 1D SRA results are in exact agreement with the reference 2D plane wave solution both in terms of wave amplitude and wave arrival time at different depths of the domain.

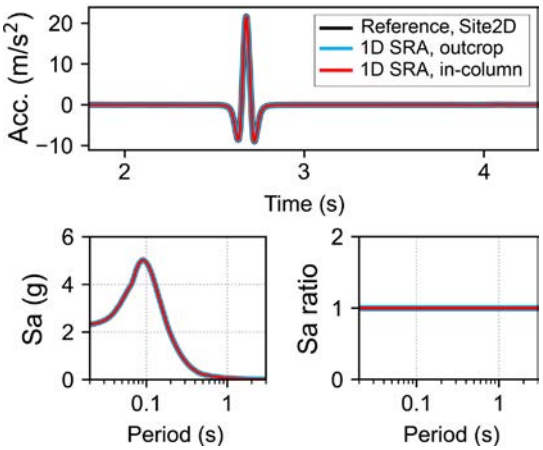

Figure. 9. Comparison of horizontal surface acceleration and its response spectra computed by 1D SRA and the reference 2D plane wave solution (incident angle=0°). Sa ratios are of the 1D predictions to the reference 2D plane wave solution.

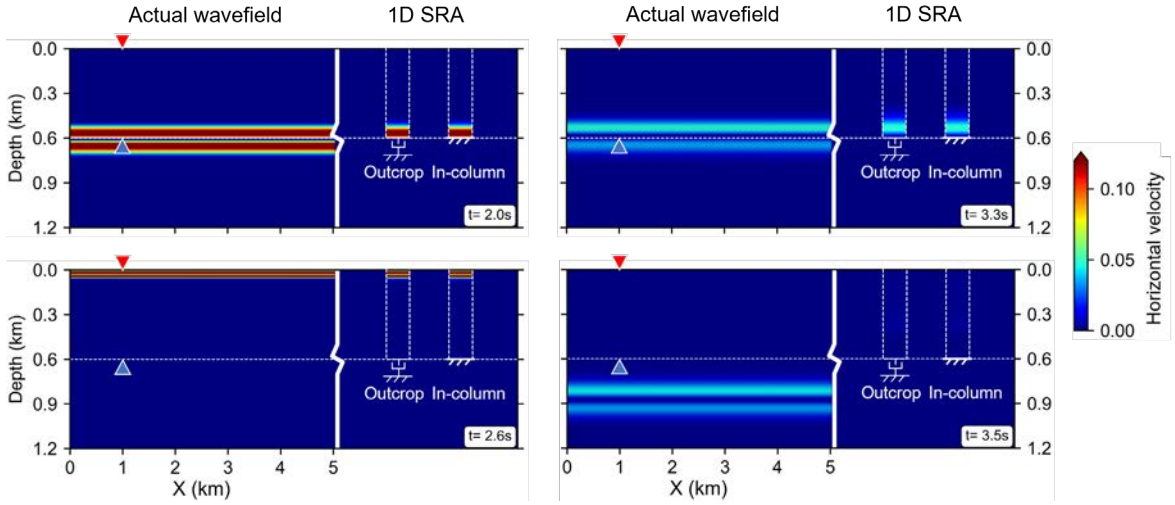

Figure. 10. Snapshots of the actual 2D wavefield (incident angle=0°) and 1D wavefields predicted by 1D SRA. Red and blue triangles denote the observation site and reference level for the 1D SRA analyses, respectively.

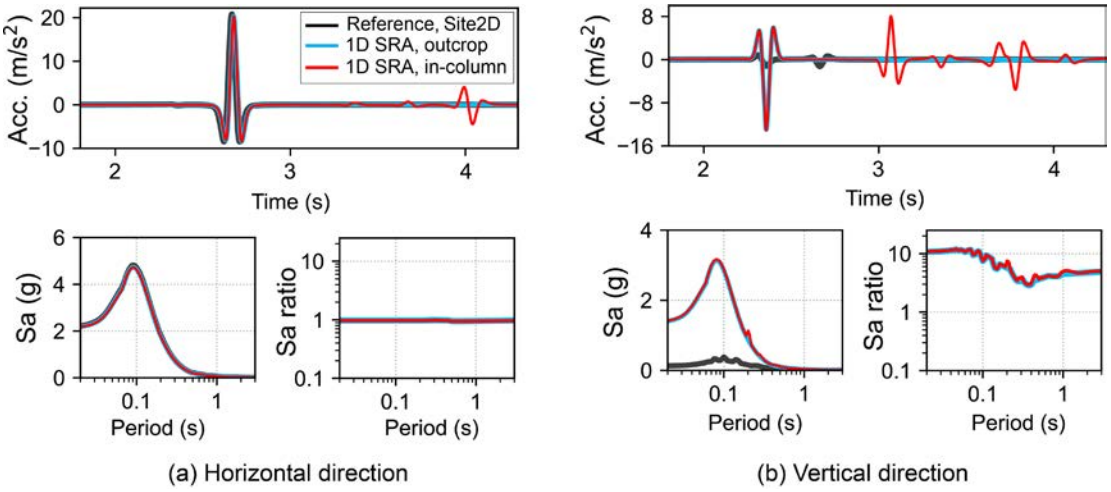

Figure. 11. Comparison of surface acceleration and its response spectra computed by 1D SRA and the reference 2D plane wave solution (incident angle=20°): (a) horizontal direction, and (b) vertical direction. Sa ratios are of 1D predictions to the reference 2D solution.

Next, we consider incident inclined SV waves impinging on the layered system. Without loss of generality, we consider an incoming SV wave incident at 20°. Figure 11 shows the comparison of horizontal and vertical surface motions from the reference 2D plane wave solution and 1D SRA predictions. In this case, the reference horizontal surface motion is dominated by the S wave arrival at 2.7s, while the reference vertical surface motion have two main wave arrivals—first converted P wave arrival at 2.4s and second S wave arrival at 2.7s. As can be seen, except for a later arriving reverberation when using the in-column motion, at this intermediate incident angle, the major horizontal motion incurred by the inclined SV wave is well captured by 1D SRA with both types of input motions.

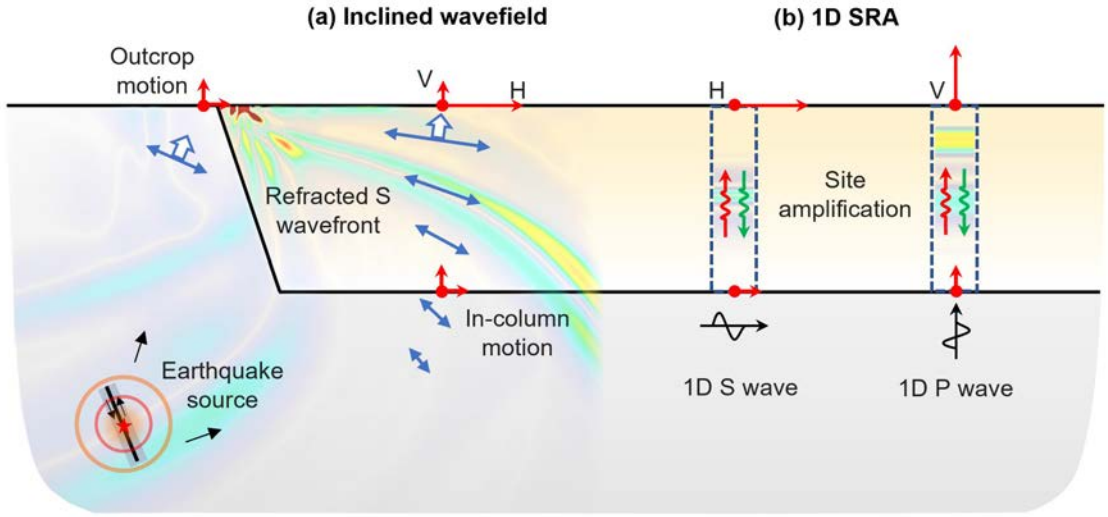

Figure. 12. Schematic of the refraction process of inclined shear waves in the surficial soft layers compared with the surface motion predictions by 1D SRA for the horizontal and vertical components.

In the vertical direction, however, apart from the extra reverberations when using the in-column motion, the vertical surface motion is significantly over-predicted by the 1D approach with the two types of input motions due to the large P wave pulse predicted by the 1D vertical P wave propagation model. This observation can be explained by the refraction process of the inclined SV wave when propagating through the soft layers, as shown schematically in Figure 12. Due to the velocity gradient of the soil profile, the wavefront of the inclined S wave is gradually refracted towards the vertical direction before reaching the surface, resulting in a tendency for increasing amplitude in the horizontal motion and decreasing amplitude in the vertical motion. This leads to decreasing amplitude ratios of the vertical motion to the horizontal motion (V/H ratio) as the shear wave propagates towards the ground surface. On the contrary, in the simplified 1D approach, since the input vertical motions were obtained when the incident inclined S wave has a relatively large vertical component, for both cases of in-column motion at depth or the surface outcrop motion, this approach will tend to over-predict the vertical motion at the surface. Additionally, the vertical motion from the 1D SRA is also subject to additional local site amplification for the assumed P waves. These combined features—the diminishment of the vertical component of the 2D wavefield due to refraction, and the amplification of the input vertical motion in the 1D SRA—result in the significant over-prediction of vertical motion from the 1D SRA. The root cause is the misrepresentation of the vertical component of motion from the incident shear wave at depth as a vertical P wave in the 1D SRA, the mechanics of this representation is simply wrong. Figure 13 shows snapshots

of the actual 2D reference wavefield and 1D wavefields predicted by 1D SRA at four instants in time. As can be seen, both the horizontal and vertical motions of the actual wavefield in the soil layers are dominated by the inclined SV wave; while the horizontal component is amplified with increasing elevation, the vertical component decreases as it approaches the surface. This is not represented in the corresponding 1D analyses, as both ground motion components are amplified in the individual site response analysis. The refraction process of the SV wave and decreasing V/H ratios with increasing elevation are also illustrated by the variation of motion through the height of soil column as shown in Figure 14.

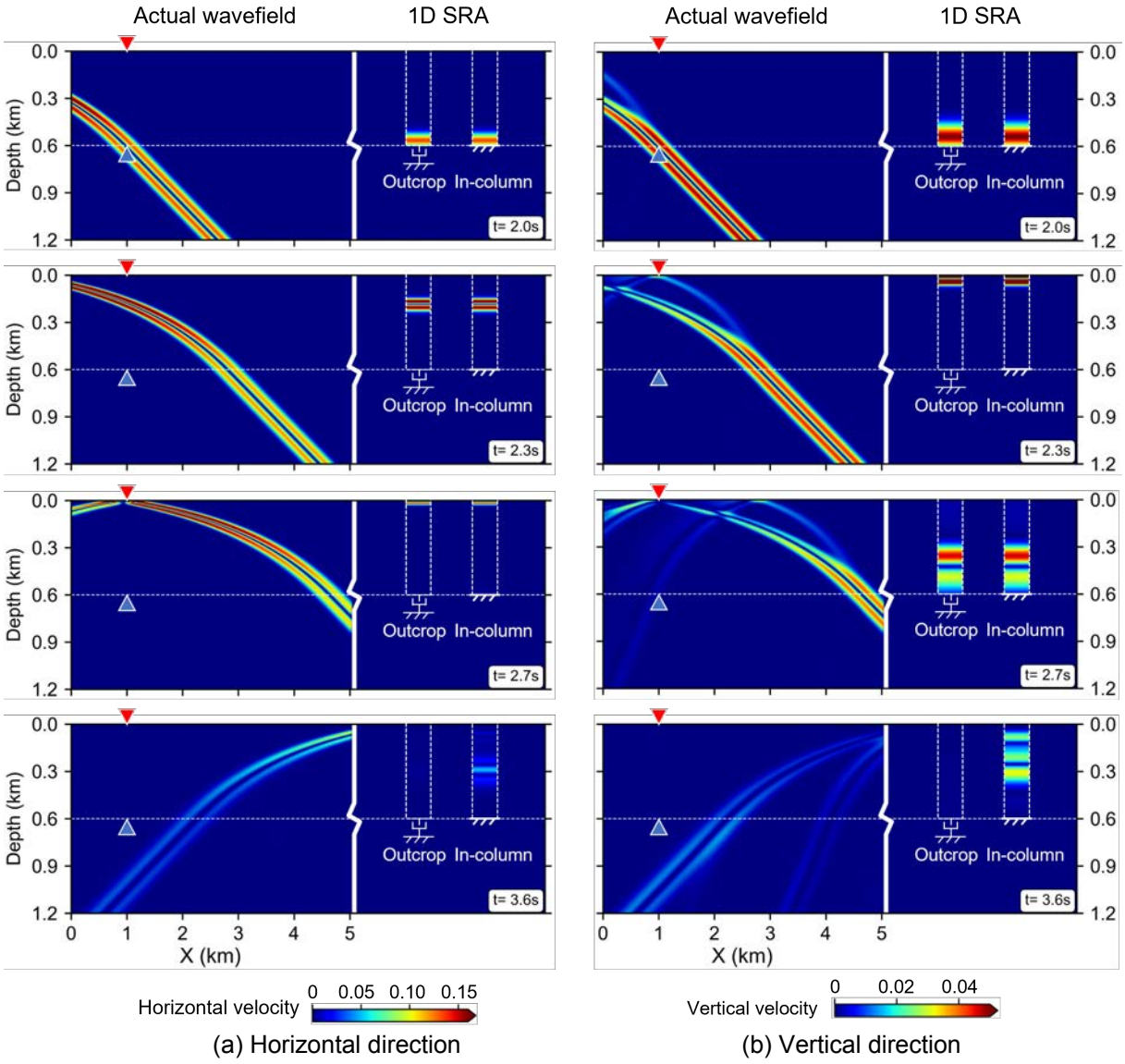

Figure. 13. Snapshots of the actual 2D inclined wavefield (incident angle=20°) and 1D wavefields predicted by 1D SRA with outcrop and in-column motions. Red and blue triangles denote the observation site and reference level for the 1D SRA analyses, respectively.

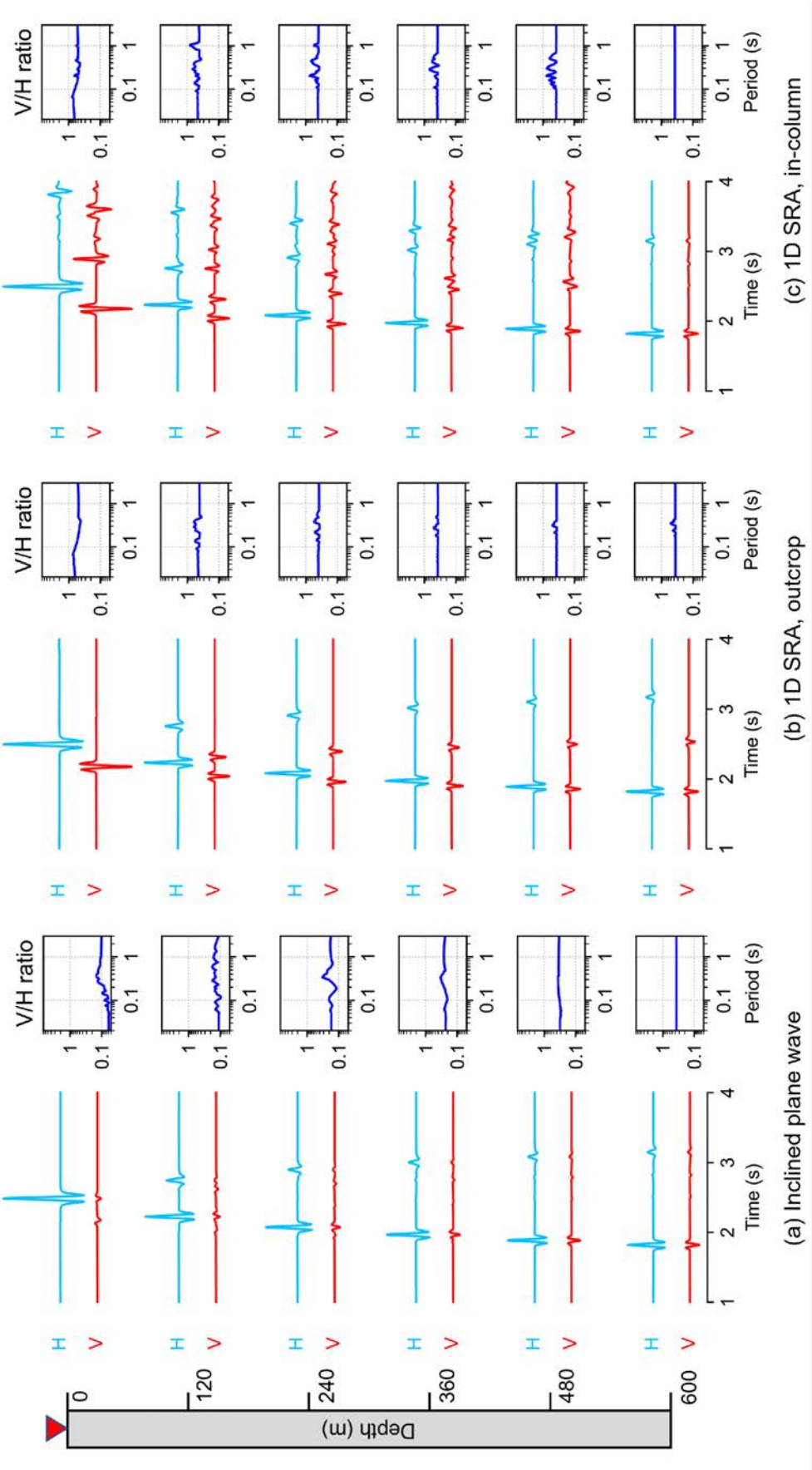

Figure. 14. Acceleration time histories and vertical-to-horizontal spectral acceleration (V/H) ratios along the depth of the surficial soft layers obtained from the (a) actual 2D inclined wavefield, (b) 1D SRA using outcrop input motion, and (c) 1D SRA with in-column input motion, for the case shown in Figure 11 (incident angle=20°). H denotes the horizontal component, and V denotes the vertical component. Note all time histories are plotted on the same scale.

3.2 Excessively long duration motion predicted with in-column input motion

As noted in the previous section, surface ground motions predicted by 1D SRA with in-column motion are observed to have excessively long duration, characterized by the multiple reverberations in the soil column in the later phases (Figure 11). Similar spurious resonances in 1D SRA based on field data have been mentioned in the existing literature [1,34]. In this section, we provide a physical explanation for this phenomenon when applying 1D SRA to inclined wavefields, as shown in Figure 15. Idealizing the motions incurred by inclined waves as either vertically propagating S or P waves lead the waves to travel different paths and even at different speeds than in reality, resulting in differences in the wave arrival time and amplitude at the 1D soil column base. Since the column base is fixed when performing the in-column 1D SRA analysis, the outgoing waves are not appropriately cancelled by the waveforms specified at the boundary, leading to spurious reflections and trapped energy that pollutes the numerical solution. If the boundary is silent when the outgoing waves arrive, this will lead to total reflection at the base. Furthermore, the wave phases in the in-column input motion that corresponds to outgoing waves in the actual inclined wavefield will serve as effectively extra input sources for the soil column. Therefore, the multiple reverberations observed in the in-column input case are a combined effect of trapped outgoing waves and spurious excitation at the base in the later phases. It should be noted that this phenomenon is more significant in the vertical direction because of the difference in the assumed wave speed (i.e., P wave speed instead of the S wave speed) and wave attenuation rate that can lead to more complex wave interferences in the 1D column.

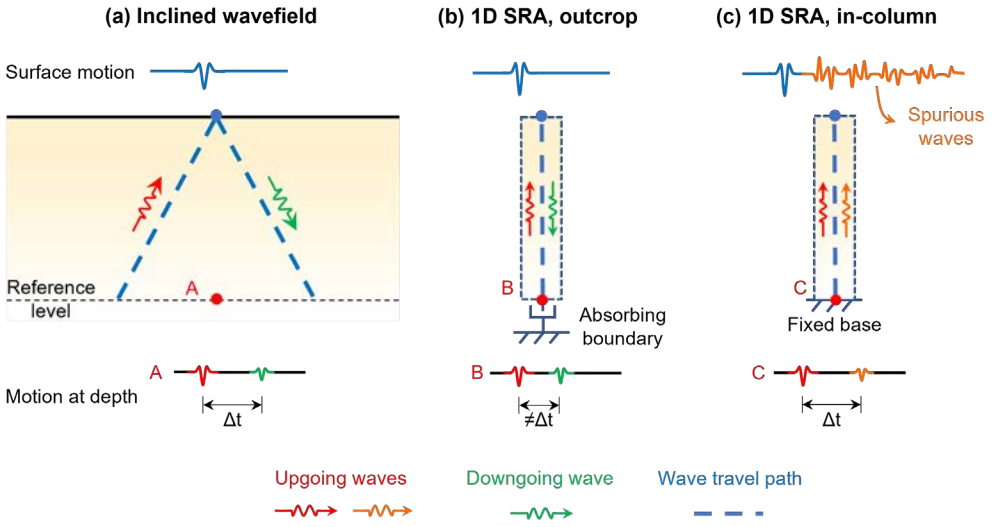

Figure. 15. Spurious waves in the 1D SRA calculation with in-column motion due to a combined effect of trapped outgoing waves and spurious input sources at the base

For demonstration purposes, we provide a simple example where 1D SRA is applied to predict the vertical ground response for an incident inclined SV wave propagating in a homogeneous half-space. The half-space has P and S wave speeds as 600m/s and 1200m/s, respectively, and the SV wave incident angle is chosen as 50° such that the converted P wave is exponentially decaying with depth to facilitate our interpretation. Figure 16 shows snapshots of the actual inclined wavefield and 1D SRA predictions at four instants of time. At t=2s, the incident wave first reaches the bottom of soil column (blue triangle), leading to the excitation of the column; at t=2.6s, the incident inclined wave reaches the surface of the column (red triangle) while the vertical P waves in the 1D analyses have already been reflected and are travelling downward; at t=3.3s, the reflected inclined SV wave reaches the column base, while the first P wave pulse in the in-column case has finished the total reflection at the base and is propagating upward, and a second upgoing P wave pulse corresponding to the reflected

inclined SV wave is beginning to be introduced into the 1D domain; at t=4s, the inclined wavefield is leaving the whole domain, while the two P wave pulses are trapped in the soil column for a long duration due to the silent boundary afterwards.

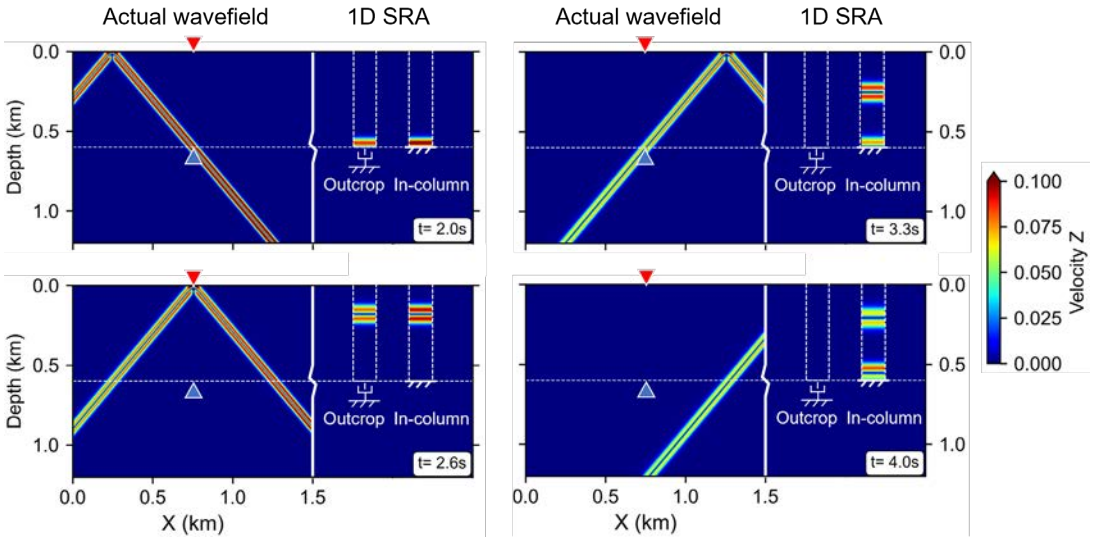

Figure. 16. Snapshots of the actual 2D inclined SV wavefield and corresponding vertical motions predicted by 1D SRA with outcrop and in-column motions. Red and blue triangles denote the observation site and reference level for the 1D SRA analyses, respectively.

4 ASSESSMENT OF 1D SRA COMPARED TO REFERENCE THREE-DIMENSIONAL GROUND MOTION SIMULATIONS

4.1 Point earthquake source scenario

For clarity of understanding, the 1D SRA results based on the analytical 2D plane waves in the previous section have intentionally focused only on incident inclined SV waves. Since incident waves from real earthquakes are composed of both P and SV waves, in this section we are particularly interested in examining the implication of applying 1D SRA to a combined P-SV incident wavefield and its potential site dependency. Considering the radiation pattern of the dip-slip point source we have used, we focus our study on the two observation sites located on the middle dashed line in the basin, as shown in Figure 5 (a). Site A is 1km from the basin edge with a calculated wave incident angle of 10.5°; site B is 4km from the basin edge with a calculated wave incident angle of 36.5°.

We perform 1D SRA for the two sites using both outcrop and in-column motions on the full-depth soil column in the basin, as mentioned earlier. Figures 17~18 show the comparison of horizontal and vertical surface motions from the reference 3D SW4 simulation and 1D SRA predictions at sites A and B, respectively. Since the horizontal motions are dominated by the major S wave arrival emitted from the point source, the horizonal components at both sites are captured reasonably well with the simplified 1D approach, although spurious reverberations with the in-column motion at site B are also apparent. Differences in the accuracy of 1D SRA can be observed in the vertical motion prediction at the two sites, especially in terms of the spectral acceleration comparison: compared to site A, the vertical motion at site B is significantly over-predicted. This is explained by the fact that the vertical motion is controlled by the early arriving P wave at 3.4s at the near-epicenter site A, while it is controlled by the late arriving SV wave at 5.7s for the farther away site B. Note that at both sites, the vertical motions in the SV window are over-predicted when assuming vertical P wave propagation for the incident inclined SV waves, and the spurious reverberations predicted with the in-column motion lead to substantial amplification near the first vibration period of the soil column (T_1=1.1s).

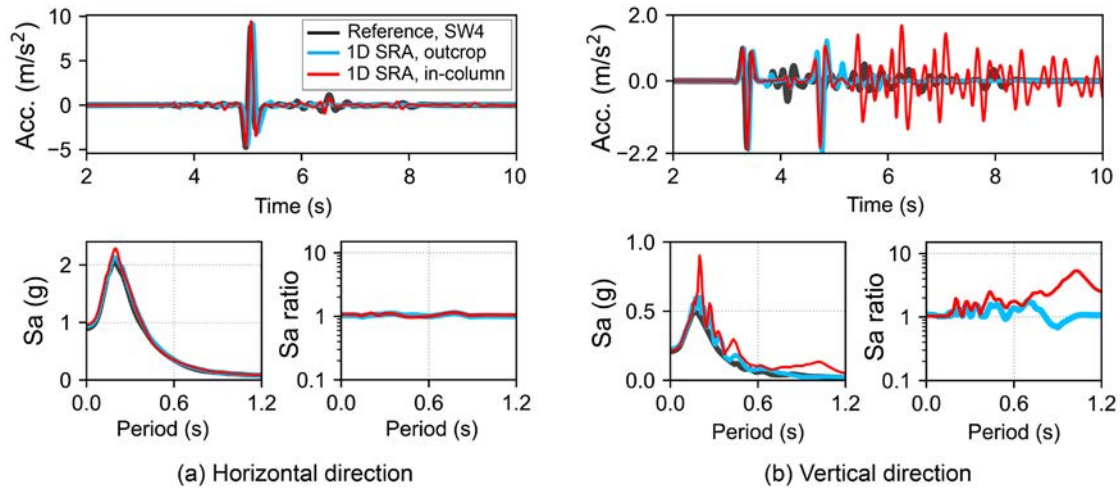

Figure. 17. Comparison of surface acceleration and its response spectra computed by 1D SRA and the reference 3D SW4 simulation for site A (incident angle=10.5°): (a) horizontal direction, and (b) vertical direction. Sa ratios are of the 1D predictions to the reference 3D solution.

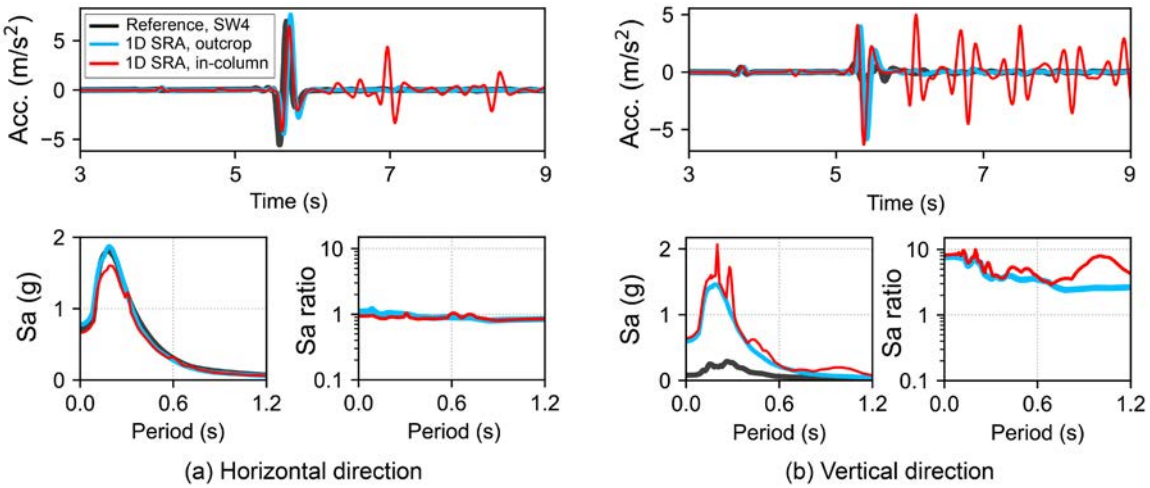

Figure. 18. Same as Figure 17 except the results are for site B (incident angle=36.5°).

To demonstrate the difference between the actual 3D wavefield simulated in SW4 and the 1D wavefields predicted by 1D SRA, we show in Figures 19-20 the accelerations and V/H ratios along the depth of the soil layers for sites A and B, respectively. From Figure 19, we see good agreement between the 3D wavefield and 1D wavefields for horizontal motions in the SV wave window, and for vertical motions in the P wave window. However, as mentioned earlier, the actual vertical motion in the SV wave window is mainly the vertical component of the inclined SV wave and decreases when the SV wavefront is refracted towards the vertical direction, while in 1D SRA, the vertical motions in the SV window have independent P wave amplification processes when propagating through the soft layers which leads to significantly larger vertical motions at the surface. Since the vertical motion amplitude is controlled by the first P wave at site A, the actual V/H ratios along depth remain rather constant and in fair agreement with the 1D predictions. Similar observations are made at site B, except the vertical motions are dominated by the incident inclined SV wave. As a result, the actual V/H ratios decrease when approaching the surface which is not captured in the 1D analyses. These observations point towards a degree of site-specificity with respect to the accuracy of 1D SRA, which has implications for universal application of the empirical V/H ratio corrections for vertical motions.

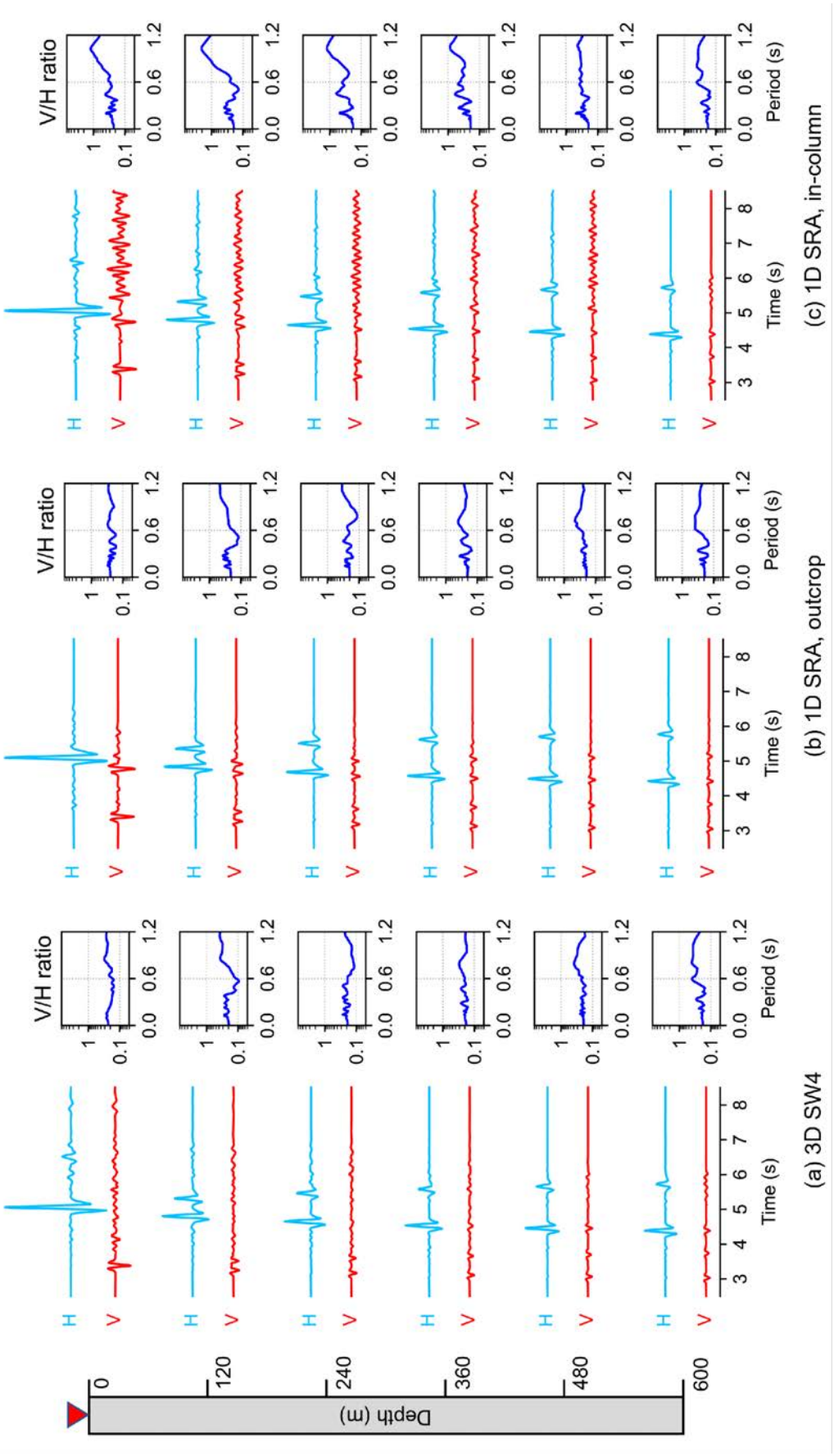

Figure. 19. Acceleration time histories and vertical-to-horizontal spectral acceleration (V/H) ratios along the depth of the surficial soft layers obtained from the (a) 3D SW4 simulation, (b) 1D SRA using outcrop input motion, and (c) 1D SRA with in-column input motion, for site A (1km from the epicenter, incident angle=10.5°). H de-notes the horizontal (radial) component, and V denotes the vertical component. Note all time histories are plotted on the same scale.

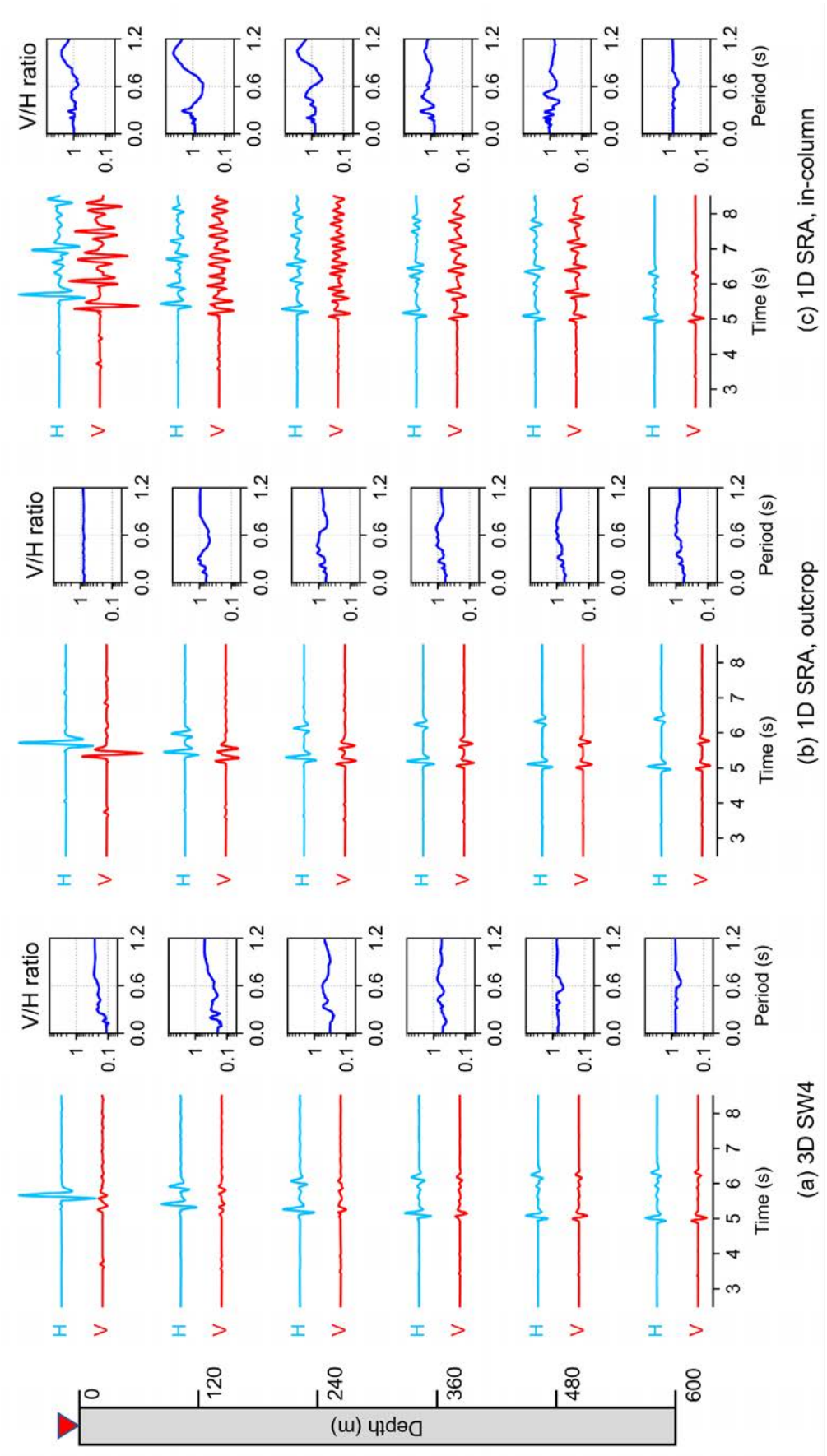

Figure. 20. Same as Figure 19 except waveforms and V/H ratios are for site B (4km away from the epicenter, incident angle=36.5°).

4.2 Broadband full 3D simulation of an extended source Mw 6.5 strike-slip event

To assess the validity of the 1D assumption when applied to complex seismic wavefields incurred by real large earthquakes, we used the representative regional model in Figure 6 as a testbed and performed broadband fully deterministic 3D earthquake simulations to obtain the reference true 3D site response solution in the whole domain. The potential implications for seismic hazard and risk assessment on a regional scale are then demonstrated through detailed site-to-site comparisons between the 3D and 1D analyses.

Horizontal and vertical surface motions at all the 602 soil sites in the sedimentary basin were predicted by the 1D approach using the simulated outcrop and in-column motions, leading to a total of 3612 site response analyses. Figure 21 shows the comparison between surface motions obtained from the 3D SW4 simulation and predictions by 1D SRA in the fault-normal (FN), fault-parallel (FP), and vertical directions at two representative sites as shown in Figure 6. At site A, the two horizontal motions are reasonably predicted by 1D SRA both in terms of waveforms and spectral acceleration. In the vertical direction, however, except for the early P wave arrivals, the vertical motions predicted by the 1D P wave propagation model is not consistent with, and is significantly larger, than the reference 3D SW4 motion in the S wave window. Note the periods of the first horizontal and vertical vibration modes of the soil column are 3.4s and 1.6s, respectively. As demonstrated in the previous sections, ground responses near the vibration periods of the soil column are amplified due to the trapped energy in the soil column when using the in-column motion and is most pronounced in the vertical direction. Compared to site A, site B is located near the basin edge (1km away) and is subjected to the strong basin-edge generated surface waves. As expected, 1D SRA with both outcrop and in-column motions were not able to capture the surface waves which leads to significantly shorter-duration motions with the outcrop motions and more severe energy trapping in both the horizontal and vertical directions when using the in-column motions.

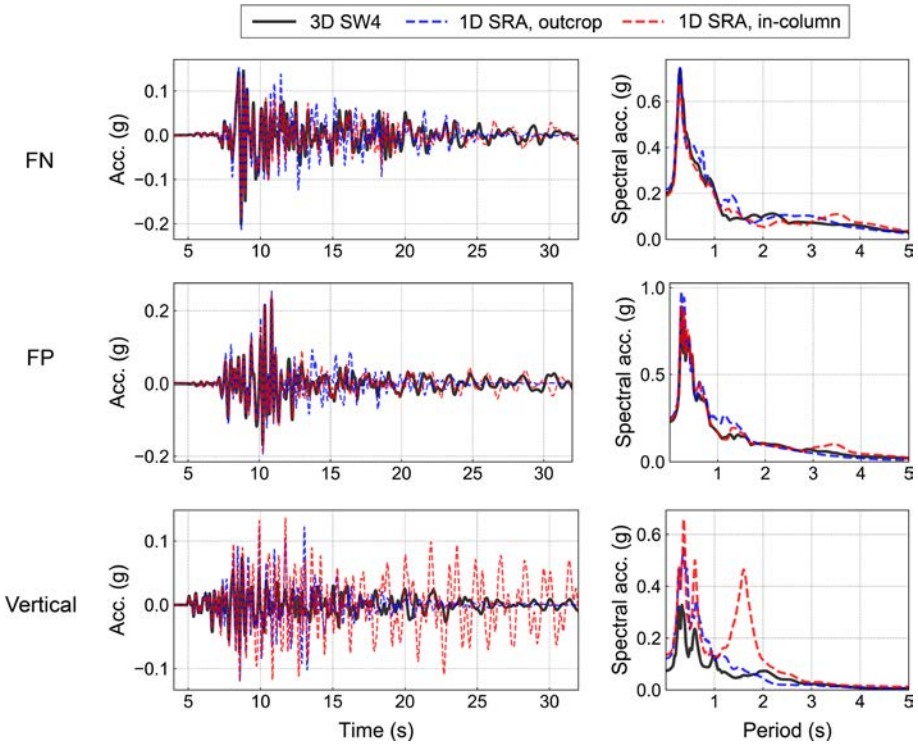

(a) Site A (7km from the basin edge)

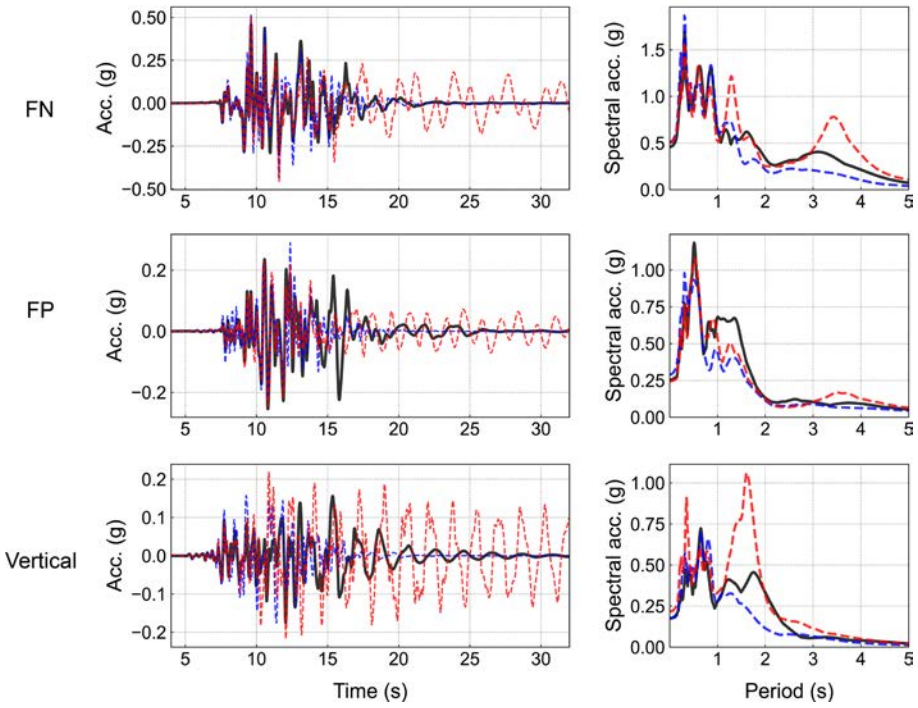

(b) Site B (1km from the basin edge)

Figure. 21. Comparison of surface motions computed by the 3D SW4 simulation and 1D SRA in the FN, FP and vertical directions for site A (a) and site B (b) show in Figure 6.

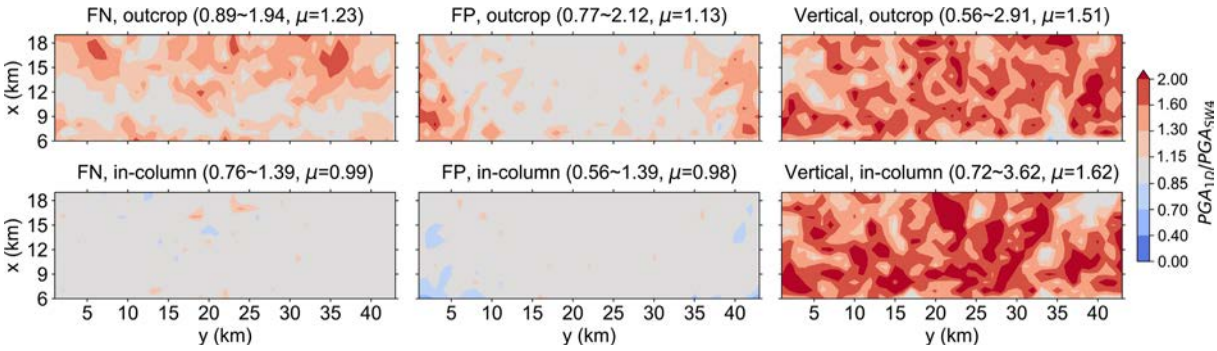

Figure. 22. PGA ratios of 1D SRA predictions to the reference 3D SW4 solution for surface motions in FN, FP and vertical directions when using outcrop motions (top row) and in-column motions (bottom row). The values in the parenthesis for each subplot are the minimum, maximum, and geometric mean of the ratios, respectively.

Ground motions at a given site in the domain are influenced by the complex 3D wave propagation phenomena. Since the 1D approach is not constructed to capture the 3D effects, the performance of the 1D approach is expected to vary from site to site. Figure 22 shows the spatial variation of the PGA ratios of the 1D SRA predictions to the 3D SW4 solution in three components using the two types of input motions. It is seen from Figure 22 that the PGA ratios of horizontal motions are reasonably well captured by the 1D approach, especially with the in-column input motion. The spatial scattering of the PGA ratios with outcrop motions may have been caused by the difference in the incident wavefield at the sites due to the change in the geologic model from which the outcrop input motions were obtained. However, in the entire computational domain, PGA of vertical motions is systematically over-predicted by an average of 50~60% when using the 1D approach. This suggests that, for realistic seismic wavefields, the ground motion amplification mechanism in the vertical direction is significantly different from that of vertical P wave propagation as assumed in 1D SRA. This obser-

vation is also confirmed in the spectral acceleration ratios for all sites considered in the domain, as shown in Figure 23. As can be seen, compared to the horizontal motions, the vertical motions are over-estimated by 1D SRA across a wide period range and by a large margin, especially near the vibration periods of the 1D soil column when using the in-column motions. It should be noted that the average SA ratios in the vertical direction are smaller than observations made in the previous sections, which can be attributed to the small velocity gradient in the basin and strong S-to-P conversions at the rock-basin interface due to the large impedance contrast we have employed in this specific example.

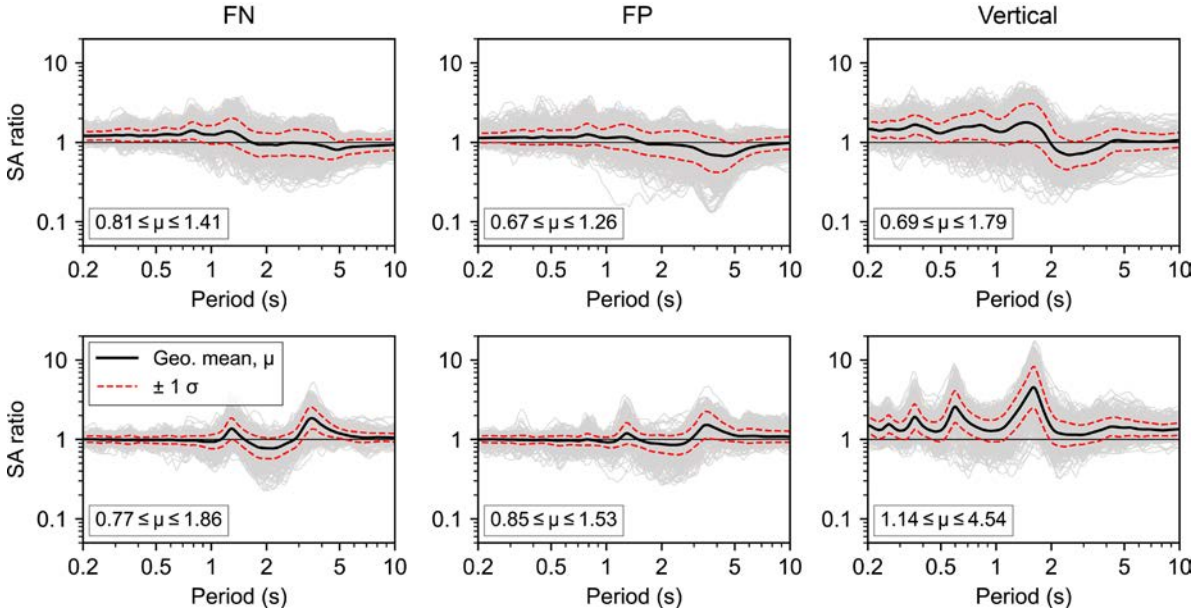

Figure. 23. SA ratios of 1D SRA predictions to the reference 3D SW4 solution for surface motions in FN, FP and vertical directions when using outcrop motions (top row) and in-column motions (bottom row).

Apart from the amplitude, strong motion duration is also important in assessing the severity of seismic risk posed to engineering systems. Figure 24 shows the ratio of 5-95% significant duration $D_{s5\text{-}95}$ between 1D predictions and 3D SW4 motions. The significant duration of surface ground motions predicted by 1D SRA with outcrop input motions is shorter than the 3D reference solution due to its inability to capture the later arriving basin-edge generated surface waves. On the other hand, the significant duration predicted by the in-column input motions are longer than the 3D reference solution due to the previously described trapped waves in the fixed-base column.

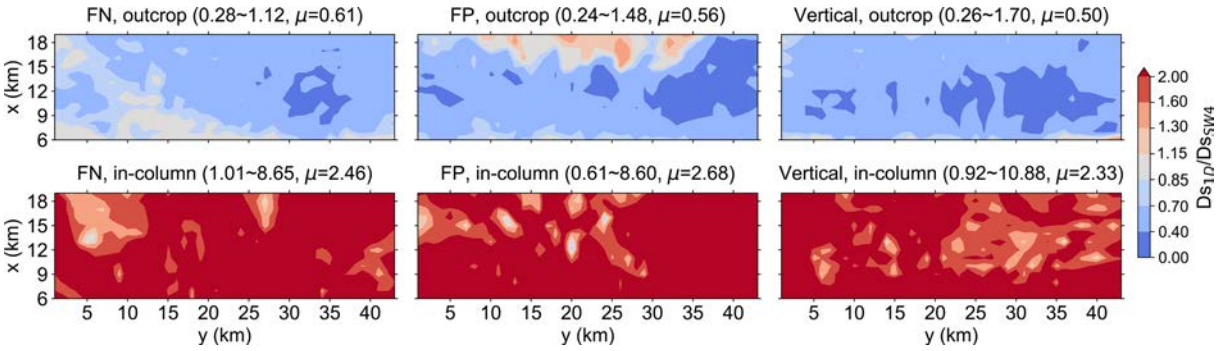

Figure. 24. Significant duration ($D_{s5\text{-}95}$) ratios of 1D SRA predictions to the reference 3D SW4 solution for surface motions in FN, FP and vertical directions when using outcrop motions (top row) and in-column motions (bottom row). The values in the parenthesis for each subplot are the minimum, maximum, and geometric mean of the ratios, respectively.

5 CONCLUSIONS

1D SRA is currently used as a standard practice in various engineering applications. In this study, we evaluate the accuracy and implications of 1D SRA when applied to general inclined seismic waves. Both analytical 2D inclined P-SV waves and realistic seismic wavefields from 3D earthquake simulations are considered. Deficiencies of the 1D approach are identified and its modeling bias for the vertical motions is highlighted. The main outcomes are summarized as follows:

(1) When the incoming vertical motion is dominated by large-amplitude inclined shear waves, the 1D approach can lead to significant over-prediction of the vertical motion due to its inability to represent the wave refraction process in the surficial soft layers. This provides insight into the over-prediction of vertical motions commonly observed in the field. Moreover, the refraction process of SV waves leads to increasing V/H ratios with depth which have been observed with field data [14].

(2) The vertical amplification mechanism is fundamentally different from that assumed in the simplified 1D approach, and the incident angle of seismic waves needs to be empirically accounted for or explicitly modeled in vertical ground motion assessment, even for small incident angles where the 1D assumption approximately holds for the horizontal motions.

(3) 1D SRA using in-column input motion can result in erroneous predicted motions with excessively long duration due to the enforced fixed boundary condition at the base of the 1D soil column that is not able to cancel the outgoing waves appropriately. This phenomenon is more problematic for vertical motion predictions since differences in the assumed wave attenuation rate and wave speed (i.e., use P wave velocity for propagating S waves) can potentially lead to more complex constructive and destructive wave interferences.

This study is a first attempt to examine the applicability of the 1D assumption with high-fidelity simulated ground motions and provide understanding of the mechanistic inconsistencies of 1D SRA. More extensive investigations and parametric exploration of the influence of earthquake source and geologic structure are underway based on large-scale 3D simulations to verify and generalize the observations made in this study.

ACKNOWLEDGEMENTS

This research was supported by the Exascale Computing Project (ECP), Project Number: 17-SC-20-SC, a collaborative effort of two U.S. Department of Energy (DOE) organizations - the Office of Science and the National Nuclear Security Administration. Computer access and exceptional support from the National Energy Research Scientific Computing Center (NERSC) at Lawrence Berkeley National Lab is gratefully acknowledged. Dr. Arben Pitarka of Lawrence Livermore National Laboratory provided input on the Graves-Pitarka kinematic rupture model for the extended source earthquake representation which is gratefully acknowledged.

REFERENCES

1. Kramer SL. *Geotechnical earthquake engineering*. Upper Saddle River, NJ, USA: Prentice-Hall; 1996.
2. Kanai K. The effect of solid viscosity of surface layer on the earthquake movements. *Bull Earthq Res Inst* 1950; 28(1): 31–35.

3. Idriss IM, Seed HB. Seismic response of horizontal soil layers. *Journal of the Soil Mechanics and Foundations Division* 1968; 94(4): 1003–1031.
4. Schnabel P, Seed HB, Lysmer J. Modification of seismograph records for effects of local soil conditions. *Bulletin of the Seismological Society of America* 1972; 62(6): 1649–1664. DOI: 10.1785/BSSA0620061649.
5. Thompson EM, Baise LG, Tanaka Y, Kayen RE. A taxonomy of site response complexity. *Soil Dynamics and Earthquake Engineering* 2012; 41: 32–43. DOI: 10.1016/j.soildyn.2012.04.005.
6. Pilz M, Cotton F. Does the One-Dimensional Assumption Hold for Site Response Analysis? A Study of Seismic Site Responses and Implication for Ground Motion Assessment Using KiK-Net Strong-Motion Data. *Earthquake Spectra* 2019; 35(2): 883–905. DOI: 10.1193/050718EQS113M.
7. Elgamal A, He L. Vertical Earthquake Ground Motion Records: An Overview. *Journal of Earthquake Engineering* 2004; 8(5): 663–697. DOI: 10.1080/13632460409350505.
8. Mok CM, Chang CY, Legaspi DE. Site Response Analyses of Vertical Excitation, *Geotechnical Earthquake Engineering and Soil Dynamics III*. Reston, VA: ASCE; 1998.
9. Tsai CC, Liu HW. Site response analysis of vertical ground motion in consideration of soil nonlinearity. *Soil Dynamics and Earthquake Engineering* 2017; 102: 124–136. DOI: 10.1016/j.soildyn.2017.08.024.
10. American Society of Civil Engineers. *Seismic Design Criteria for Structures, Systems, and Components in Nuclear Facilities*. ASCE/SEI 43-05. Reston, VA: American Society of Civil Engineers; 2005.
11. American Society of Civil Engineers. *Seismic Analysis of Safety-Related Nuclear Structures*. ASCE/SEI 4-16. Reston, VA: American Society of Civil Engineers; 2017.
12. American Society of Civil Engineers. *Minimum Design Loads and Associated Criteria for Buildings and Other Structures*. ASCE/SEI 7-16. Reston, VA: American Society of Civil Engineers; 2017. DOI: 10.1061/9780784414248.
13. McGuire RK, Silva WJ, Costantino CJ. *Report NUREG/CR-6728: Technical Basis for Revision of Regulatory Guidance on Design Ground Motions: Hazards- and Risk-Consistent Ground Motion Spectra Guidelines*. Washington DC, USA: US Nuclear Regulatory Commission; 2001.
14. Ostadan F, Deng N. *Advanced Nuclear Technology: Modeling Vertical Free-Field Motion for Soil-Structure Interaction of Embedded Structures*. Palo Alto, CA: EPRI; 2018.
15. Chao SH, Lin CM, Kuo CH, Huang JY. Dominant Waves in Vertical Ground Motion in Taiwan, Taipei, Taiwan: National Center for Research on Earthquake Engineering; 2020.
16. Cabas A, Carcamo P, Rodriguez-Marek A, Godfrey B, Olgun G. Where to Locate the Elastic Half-Space in Site Response Analysis, A Case Study Using Site Profiles from Charleston, SC, USA, *Proc. 2nd European Conference on Earthquake Engineering and Seismology*. Istanbul, Turkey: 2014.
17. McCallen D, Petersson A, Rodgers A, *et al.* EQSIM—a Multidisciplinary Framework for Fault-to-Structure Earthquake Simulations on Exascale Computers Part I: Computational Models and Workflow. *Earthquake Spectra* 2021; 37(2): 707–735. DOI: 10.1177/8755293020970982.
18. Petrone F, Abrahamson N, McCallen D, Pitarka A, Rodgers A. Engineering Evaluation of the EQSIM Simulated Ground-Motion Database: The San Francisco Bay Area Region. *Earthquake Engineering & Structural Dynamics* 50(15): 3939–3961. DOI: 10.1002/eqe.3540.
19. Aki K, Richards PG. *Quantitative Seismology*. 2nd ed. Mill Valley, California: University Science Books; 2009.

20. Zhao W, Chen W, Yang D, Tan X, Gao H, Li C. Earthquake input mechanism for time-domain analysis of tunnels in layered ground subjected to obliquely incident P- and SV-waves. *Engineering Structures* 2019; 181: 374–386. DOI: 10.1016/j.engstruct.2018.12.050.
21. Borcherdt R. Inhomogeneous body and surface plane waves in a generalized viscoelastic half-space. 1971.
22. Krebes ES, Daley PF. Difficulties with computing anelastic plane-wave reflection and transmission coefficients. *Geophysical Journal International* 2007; 170(1): 205–216. DOI: 10.1111/j.1365-246X.2006.03349.x.
23. Python Software Foundation. multiprocessing — Process-based parallelism. *Python Documentation*. https://docs.python.org/3/library/multiprocessing.html [accessed February 16, 2023].
24. Lam SK, Pitrou A, Seibert S. Numba: a LLVM-based Python JIT compiler. *LLVM '15: Proceedings of the Second Workshop on the LLVM Compiler Infrastructure in HPC*, New York, NY, United States: Association for Computing Machinery; 2015. DOI: 10.1145/2833157.
25. McCallen D, Tang H, Wu S, Eckert E, Huang J, Petersson NA. Coupling of regional geophysics and local soil-structure models in the EQSIM fault-to-structure earthquake simulation framework. *The International Journal of High Performance Computing Applications* 2022; 36(1): 78–92. DOI: 10.1177/10943420211019118.
26. Zhang W, Taciroglu E. 3D time-domain nonlinear analysis of soil-structure systems subjected to obliquely incident SV waves in layered soil media. *Earthquake Engineering & Structural Dynamics* 2021; 50(8): 2156–2173. DOI: 10.1002/eqe.3443.
27. Wolf JP, Obernhuber P. In-plane free-field response of actual sites. *Earthquake Engineering & Structural Dynamics* 1983; 11(1): 121–134. DOI: 10.1002/eqe.4290110110.
28. Hashash Y, Musgrove M, Harmon J, *et al. DEEPSOIL 7, User Manual*. Urbana, IL, Board of Trustees of University of Illinois at Urbana-Champaign; 2020.
29. Mazzoni S, McKenna F, Scott MH, Fenves GL. *OpenSees Command Language Manual*. University of California, Berkeley; 2006.
30. Rodgers AJ, Petersson A, Pitarka A, McCallen DB, Sjogreen B, Abrahamson N. Broadband (0–5 Hz) Fully Deterministic 3D Ground-Motion Simulations of a Magnitude 7.0 Hayward Fault Earthquake: Comparison with Empirical Ground-Motion Models and 3D Path and Site Effects from Source Normalized Intensities. *Seismological Research Letters* 2019; 90(3): 1268–1284. DOI: 10.1785/0220180261.
31. Petersson N, Sjogreen B. *User's guide to SW4, version 2.0*. Livermore, CA: Lawrence Livermore National Laboratory; 2017.
32. National Energy Research Scientific Computing Center. Cori. *NERSC Documentation*. https://docs.nersc.gov/systems/cori/ [accessed February 22, 2023].
33. Graves R, Pitarka A. Kinematic Ground-Motion Simulations on Rough Faults Including Effects of 3D Stochastic Velocity Perturbations. *Bulletin of the Seismological Society of America* 2016; 106(5): 2136–2153. DOI: 10.1785/0120160088.
34. Boore DM. The Uses and Limitations of the Square-Root-Impedance Method for Computing Site Amplification. *Bulletin of the Seismological Society of America* 2013; 103(4): 2356–2368. DOI: 10.1785/0120120283.